Bioresource Technology Reports 23 (2023) 101568

Contents lists available at ScienceDirect

Bioresource Technology Reports

journal homepage: www.sciencedirect.com/journal/bioresource-technology-reports

The production of activated carbon from *Acacia erioloba* seedpods via phosphoric acid activation method for the removal of methylene blue from water

Likius Shipwiisho Daniel [a,b,*], Ateeq Rahman [a], Mirjam Ndakola Hamushembe [a], Paulus Kapolo [a], Veikko Uahengo [a], Sreekantha Babu Jonnalagadda [c]

[a] Department of Physics, Chemistry and Material Science, University of Namibia, Postbag 13301, Windhoek, Namibia
[b] Multidisciplinary Research Service, Centre for Research Services, University of Namibia, Postbag 13301, Windhoek, Namibia
[c] School of Chemistry and Physics, University of KwaZulu-Natal, Durban 4000, South Africa

ARTICLE INFO

Keywords:
Activated carbon
Proximate analysis
Acacia seed pods
Brunauer–Emmett–Teller
Langmuir model Freundlich model
Phosphoric acid

ABSTRACT

Wastewater treatment requires a lot of granular activated carbon to absorb the dissolved organic components. This article describes a low-cost process for making highly active adsorption activated carbons from biomass, which could be used for wastewater treatment. A one-step carbonization and chemical activation with phosphoric acid at 500 °C produced low-cost acacia-derived porous activated carbons. The activated carbons' moisture, ash, volatile matter, and fixed carbon content were determined using proximate analysis. The activated carbon's adsorption qualities were also determined by studying its bulk density, surface morphology, power of hydrogen, iodine number, and methylene blue number index. To test the produced activated carbons for water treatment, batch adsorption dynamics were performed at room temperature for the removal of methylene blue from aqueous solution. Compared to activation using H_2SO_4, H_3PO_4 proves superior in generating well-developed pores, leading to a mesoporosity and microporosity structure with a larger surface area and high adsorption capacity. Brunauer–Emmett–Teller determined the sample's specific surface area, which was found to be 387 m^2/g. The iodine number for 50, 100, and 200 μm activated carbon particles size was 620, 592, and 632 mg/g, respectively. The adsorption of MB on AC material better fits with Langmuir's adsorption isotherm; hence, particles are adsorbed on well-pronounced heterogeneous surfaces. The sips model is found to best represent the equilibrium data with R^2 values of 0.994, suggesting the heterogeneous surface adsorption of MB on AC. Therefore, the adsorption of AC by MB involves physical and chemical processes. The produced AC hence appears to remove dissolved organic contaminants from raw water.

1. Introduction

The semiarid savanna grasslands and woodlands of Africa are progressively transforming into a dense, shrub-dominated landscape. Bush encroachment is the thickening and spreading of woody vegetation in open grasslands and forests. This makes it more difficult for animals to locate food (Eldridge et al., 2011). This can also make the land less suitable for farming and rearing animals (Van Auken, 2009). Degraded rangelands in African savannas have caused financial losses for commercial farmers due to the loss of grazing, arable land, and hunting grounds for animals, especially in non-migratory ranches in Southern Africa (De Wet, 2015; Ayelew and Mulualem, 2018). Several African nations are currently afflicted by bush encroachment, including South Africa, Botswana, Uganda, Zimbabwe, Ethiopia, and Namibia (Ayelew and Mulualem, 2018; Charis et al., 2019). Bush encroachment affects >30 million hectares of land in Namibia, resulting in decreased carrying capacity of the rangelands, loss of biodiversity, and, in the medium term, a decrease in available groundwater due, among other things, to the increased water uptake by the encroacher bushes (Uchezuba et al., 2019). The consequence is approximately 100 million euros in annual economic losses and a significant loss of agricultural employment (Uchezuba et al., 2019). The shrubs have generated an estimated 200 million tons of previously dormant wood biomass (Ayelew and Mulualem, 2018). By discovering new methods to utilize biomass for valuable

* Corresponding author at: Department of Physics, Chemistry and Material Science, University of Namibia, Postbag 13301, Windhoek, Namibia.
E-mail address: daniels@unam.na (L.S. Daniel).

https://doi.org/10.1016/j.biteb.2023.101568
Received 1 May 2023; Received in revised form 21 July 2023; Accepted 22 July 2023
Available online 27 July 2023

products and development, bush control projects can create jobs in agriculture and industry.

In Namibia, the available natural resources are underutilized, and their economic value is understated. A lack of scientific expertise and infrastructure to analyze locally accessible natural resources and develop novel materials is a contributing factor (Shikangalah and Mapani, 2020). The rapid growth of Acacia species poses a threat to native plants and animals, altering soil moisture and local biodiversity (De Wet, 2015). It is considered undesirable and invasive due to its thorny, fast-growing, and encroaching characteristics, especially in grassland regions (Shikangalah and Mapani, 2020). Therefore, its utilization in the production of activated carbon (AC) adsorbents could contribute to a much-needed solution for vegetation encroachment. AC can then be used as an adsorbent to purify water. AC is currently the most widely used adsorbent in both industrial and domestic applications (Joshi, 2015). AC can purify a variety of effluent types. AC is used in various industries in Namibia, including power, chemical, paper, pharmaceutical, fertilizer, and textile industries. Using encroacher vegetation from Namibia as a source of AC can aid in the restoration of degraded savanna. Currently, only a fraction of available resources is utilized, resulting in a slow rate of land restoration. *Acacia erioloba* (*A. erioloba*), a species of densely distributed invasive encroacher shrub, was chosen for the adsorbent formulation in this study.

To remove vapor organic compound (VOC) pollutants from the wastewater, techniques such as electrolysis, chemical flocculation, catalytic degradation, biofiltration, membrane separation, absorption, and adsorption have been developed (Santoso et al., 2020). Adsorption is a good method because it is simple, efficient, cost-effective, and uses low energy (Kutluay et al., 2020; Mahmood et al., 2017). Hence, AC is the most widely utilized adsorbent in companies and homes for treating various effluents (Seymour and Milton, 2003a, 2003b). Due to chronic water stress, since 1968, Windhoek, the capital of Namibia, has used treated wastewater to produce drinking water. Wastewater reuse for drinking purposes is not standard because only 4 % of sewage is generally recycled, mainly for industrial needs (Birch et al., 2016). Windhoek's Goreagab Water Reclamation plant uses advanced "multi-barrier" technologies, including powdered and granular activated carbons (200 to 5000 μm) (Maquet, 2020). Powdered AC (50–150 μm) is added to the raw water to remove algae and dissolved organic matter like humic substances, enabling the removal by enhanced coagulation and partial deactivation of harmful microbiology (Shutova et al., 2020). The remaining dissolved organic compounds in the water are then adsorbed onto the granular AC (Jjagwe et al., 2021), which demands considerable amounts of AC for wastewater treatment in Namibia. Thus the study of AC's different sizes is crucial.

The researchers have thoroughly studied the impact of processing factors like activation temperature, impregnation ratio, and soaking time on the development of porosity during the H_3PO_4 activation of lignocellulosic precursors under an inert atmosphere (El Gaayda et al., 2022; Nahil and Williams, 2012; Duan et al., 2017; Liu et al., 2014). However, the effects of different sizes of raw materials are not well presented. Moreover, to cope with the massive requirement of powdered and granular activated carbon in Namibia, AC should be produced utilizing local resources and a cost-effective method. Acacia seedpods are traditionally used to produce high-quality charcoal that burns slowly and leaves little ash (Rahman et al., 2019). Furthermore, carbon produced from acacia is more rigid and more resistant to attrition (Gratuito et al., 2008). AC can be prepared by physical or chemical activation. Physical activation involves carbonizing raw material at 400–1000 °C and then activating it using steam, carbon dioxide, air, or their mixes (Song et al., 2013). Chemical activation involves concurrent carbonization and activation. The method requires less heat, and a simple laboratory setup is sufficient with less complex operating conditions than physical activation technique (Song et al., 2013). Many researchers have prepared and characterized AC from carbonaceous materials (Gratuito et al., 2008; El-Shafey et al., *2016*; Tounsadi et al., 2016), but few have used *Acacia erioloba* seedpods (Rahman et al., 2019).

It's important to find low-cost raw materials that have similar or better characteristics than conventional ones (Dias et al., 2007). Seymour and Milton (2003a, 2003b) have reported that *A. erioloba* species burn slowly, producing little ash. Low ash production may be caused by high carbon content in *A. erioloba* species, resulting in a higher yield of AC. Since it is still a challenge to prepare AC with very specific characteristics (such as pore size distribution, carbon content, etc.), it is important to assess AC produced from different activation agents since activation agents also have different characteristics (Seymour and Milton, 2003a, 2003b). Using *A. erioloba* seedpods-based AC treated with H_3PO_4 as activation agent for water treatment is an interesting and innovative approach, especially in countries with water scarcity like Namibia. It provides new opportunities to utilize existing biomass for value creation processes in terms of value addition and product development, bush control initiatives can generate employment opportunities in both agriculture and industry. Recently, we reported the chemical preparation of AC from *A. erioloba* seedpods employing sulfuric acid (H_2SO_4) as an activation agent (Rahman et al., 2019). However, the activated carbon's specific surface area (10.13 m^2/g), and its adsorption capacity (1.45 mg/g) (Rahman et al., 2019), were very low compared to other activated carbons reported in literature (Itodo et al., 2010a, 2010b). In previous preparation of AC derived from Acacia seed ponds, 600 °C was used as a carbonization temperature (Rahman et al., 2019). Increasing carbonization temperature promoted the release of volatile matter from the raw materials (Mahari et al., 2021), the thermal stability improved (Li et al., 2017), and decreased the maximum weight loss (Jang et al., 2019). However, Puziy et al., 2020 reported that the use of phosphoric acid as an activation agent resulted in a higher amount of AC obtained at a lower temperature (500 °C) than for carbon obtained at 800 °C. The highest specific surface area (1470 cm^2/g) and total pore volume (0.60 cm^3/g) were obtained in the final porous carbon when the petroleum coke was carbonized at 500 °C, while the porosity was reduced with further increasing the carbonization temperature (Jang et al., 2019). We are now considering the use of H_3PO_4 as an activator and 500 °C as a carbonization temperature to enhance the adsorption capacity and specific surface area of *A. erioloba* seedpods-based AC. Moreover, compared to zinc chloride ($ZnCl_2$) and H_2SO_4 activation, H_3PO_4 activation provides environmental benefits, easy recovery, low energy cost, and high char yield (33. Lim et al., 2010). Chemical activation with H_3PO_4 was employed for making hemp stem-based AC because the process is quite simple (Lupul et al., 2015).

This article describes the chemical synthesis of AC using *A. erioloba* seedpods as a carbon-based precursor and H_3PO_4 as an activator. We concentrate on the utilization of economical Acacia seedpod residues as raw materials to produce activated carbons using a straightforward one-step pyrolysis process. The influence of the size of particles on the adsorption characteristics of AC is explained. Various analytical techniques were used to characterize the prepared ACs, including scanning electron microscopy (SEM) with energy dispersive spectroscopy (EDX), Brunauer–Emmett–Teller (BET), proximate analysis, adsorption kinetics and isotherms and iodine number index. This article describes a practical, low-cost procedure for preparing activated carbon from locally available biomass, with the aim to increase the adsorption capacity, specific surface area (S_{BET}), pore volume, and pore dimension of the AC derived from *A. erioloba* seedpods, now using H_3PO_4 instead of H_2SO_4.

2. Materials and methods

2.1. Chemical used

H_3PO_4 (10 %), hydrochloric acid (HCl) (0.1 M), methylene blue (MB) ($C_{16}H_{18}ClN_3S$) (0.003 M), potassium iodide (KI) (0.02 M), potassium iodate (KIO_3), sodium thiosulphate pentahydrate ($Na_2S_2O_3{\cdot}5H_2O$), sodium hydroxide (NaOH), starch and iodine were procured from Sigma-Aldrich. For all experiments, distilled water was used to prepare the

Table 1
Chemicals used in this research.

Chemical[a]	Abbreviation[b]	Conc.
Phosphoric acid	H_3PO_4	10 %
Hydrochloric acid	HCl	0.100 M
Methylene blue	MB	0.003 M
Potassium iodide	KI	0.020 M
Potassium iodate	KIO_3	0.001 M
sodium thiosulphate pentahydrate	$Na_2S_2O_3{\cdot}5H_2O$	0.100 M
Starch	$(C_6H_{10}O_5)_n$	0.139 M
Iodine	I_2	0.100 M

[a] The purchased chemicals were used without further purification.
[b] Abbreviation that are used in this paper and recognised in chemical industry.

aqueous solutions. Reactants grade H_3PO_4, KI, KIO_3, NaOH, $Na_2S_2O_3$ (purity >98 %), H_3PO_4 (purity of 85 %) and HCl (purity >37 %) were purchased and used in this experiment. Table 1 shows all chemicals that were used, all were of analytical grade and were used as received without any further purification.

2.2. Production of activated carbon

The seedpods were collected from an *A. erioloba* Camelthorn tree at the University of Namibia. The seedpods were sun-dried, crushed and ground in a ball mill to form a biomass precursor. The sample was sieved to acquire particles of uniform size, measuring between 1.0 and 1.5 mm (mm) in diameter. The precursor was rinsed with distilled water to remove surface-bound impurities and mud, and then dried for 12 h at 105 °C.

In a 500 mL flask, 25 g of the desiccated precursor was impregnated with 150 mL of 10 % phosphoric acid as an activating agent. The calculated amount of the dried Acacia seedpod powder and the activating agent were mixed, as per the impregnation ratio (IR), presented in Eq. (1).

$$\text{Impregnation ratio (I.R)} = \frac{\textit{weight of the active agent added}}{\textit{weight of the carbonizing material}}, \quad (1)$$

The flask containing the mixture was wrapped in aluminum foil and left at room temperature overnight. After submerging, the sample was first transferred to a crucible, covered with a lid and heated for 2 h at 110 °C on a hot plate. The samples were filtered using vacuum technique and rinsed with hot deionized water (approximately 80 degrees Celsius) till the pH was neutral. The material was then desiccated in an oven at 105 ± 5 °C for 24 h. The desiccated biomass was transferred into a crucible and placed in a tubular muffle furnace (OTF-1200X; Hefei Kejing Material Technology Co., Ltd.). The pyrolysis temperature was set at 500 °C with a heating rate of 5 °C·min^{-1} under the protection of a N_2 atmosphere for 1 h. The obtained sample was subsequently rinsed with 100 mL of 0.1 M HCl to remove undesirable substances, filtered by vacuum filtration, and washed with hot deionized water until the pH was neutral. The residue was desiccated in a 105 °C oven for 3 h. The biomass samples were stored in sealed vials for further analysis. Eq. (2) was used to calculate the chemical activation process's efficiency by determining the AC's chemical-free percentage yield.

$$\%Yield = \frac{M_2}{M_1} \times 100\% \quad (2)$$

Where M_1 and M_2 are the masses of the carbonized sample before and after activation, respectively.

The collected biomass sample was then sieved into three distinct particle sizes of 50, 100, and 200 μm and was designated throughout this paper as AC-1, AC-2, and AC-3, respectively. The purpose of sieving the material into three distinct particle sizes was to assess the influence of particle size on the adsorption capacity of AC. The schematic diagram for the process of preparing AC is depicted in Scheme 1. All these steps were done in triplicate to obtain the statistical data.

2.3. Ultimate and proximate analysis of the prepared activated carbon

SEM with cold emission (UHR FESEM Hitachi SU8020) evaluated AC morphologies. LECO Corporation elemental analyzers analyzed activated carbons' elemental composition. The AC-1, AC-2, and AC-3 samples were proximately analyzed in triplicate to assess pH, moisture, ash, volatile matter, bulk density, and fixed carbon (Tounsadi et al., 2016; Jagtoyen, 1996). For quantitative analysis, the pH, 0.5 g of each AC powder sample and 100 mL of distilled water in triplicate were placed in 500 mL Erlenmeyer flasks was stirred for 60 min, followed by pH measurement. For the moisture content, a 0.5 g AC sample was put into pre-weighed crucibles, in triplicate and heated in an oven at 125 °C for 90 min. The crucible was left in the furnace for overnight to cool. After cooling, the weight of the dried sample was measured. The same procedure was repeated for the AC-2 and AC-3 powders, respectively. Eq. (3) was employed (Tounsadi et al., 2016).

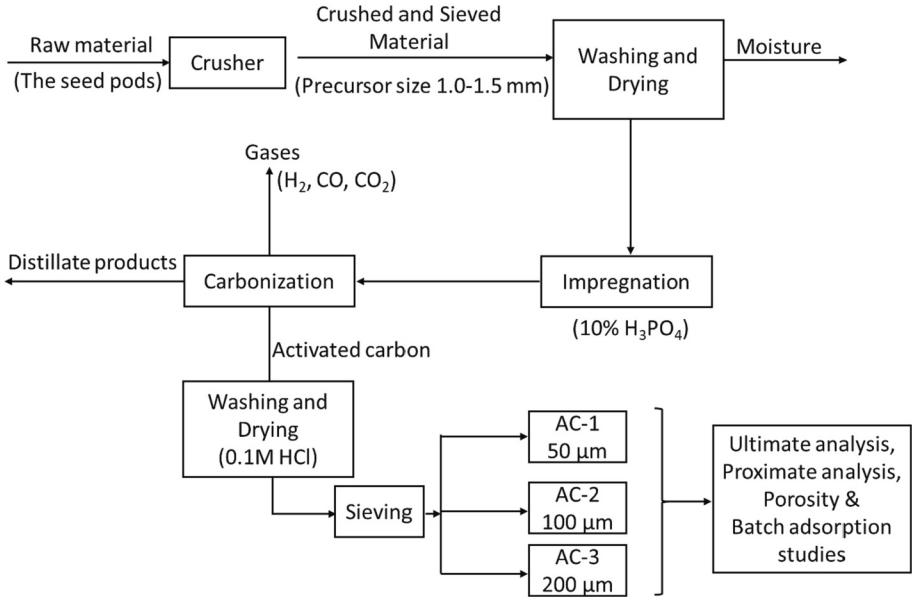

Scheme 1. The schematic diagram for preparation of activated carbon.

$$\%\text{Moisture content (M\%)} = \frac{100(B-F)}{(B-G)} \quad (3)$$

Where B = mass of crucible + original sample, F = mass of crucible + dried sample and G = mass of empty crucible.

The ash content was estimated by placing 0.5 g of AC-1, AC-2 and AC-3 powder into pre-weighed crucibles. The crucibles were heated in a muffle furnace to 750 °C for 90 min. During this heating process, the crucibles were left open. The crucibles were left to cool overnight and weighed. The procedure was repeated three times to obtain an average value. Eq. (4) was used to calculate the average ash content (Tounsadi et al., 2016)

$$\%\text{Ash content (A\%)} = \frac{100(F-G)}{(B-G)} \quad (4)$$

Where G = mass of empty crucible, B = mass of crucible + sample and F = mass of crucible+ ash sample.

A known amount of AC-1 powder was placed in a conical crucible with a lid to determine volatile matter content. It was then muffle-fired for 7 min at 925 °C. The crucible was weighed after cooling overnight. To get an average, it was carried out on three separate occasions. AC-2 and AC-3 powders were processed similarly. Eq. (5) (Tounsadi et al., 2016) was employed for this purpose.

$$\%\text{volatile matter on a dry basis (VM\%)} = \frac{100[100(B-F)-M(B-G)}{[(B-G)(100-M)} \quad (5)$$

Where B = mass of crucible, lid and sample before heating, F = mass of crucible, lid and contents after heating, G = mass of empty crucible & lid and M% = percentage of moisture determined in Eq. (3) above.

The bulk density (BD) was estimated by determining the mass of the measuring cylinder with and without 1 g of AC-1 powder sample in triplicate using Eq. (6) (Tounsadi et al., 2016). AC-2 and AC-3 powders were processed similarly.

$$BD = \frac{M_2 - M_1}{V} \quad (6)$$

Where M_1 = mass of measuring cylinder in grams, M_2 = mass of measuring cylinder + its contents and V = volume of the measuring cylinder in liters.

Finally, the fixed carbon (FC) content was determined using Eq. (7) (Tounsadi et al., 2016).

$$FC = 100–(M\% + VM\% + A\%) \quad (7)$$

2.4. Porosity study of the prepared AC based on iodine number determination

Iodine number is the amount of iodine adsorbed by one gram of adsorbent from a 0.10 M reference iodine solution when its equilibrium iodine content is 0.02 M. Herein, the iodine number quantifies the microporosity of activated carbon. A greater iodine number indicates that the sample has greater microporosity. The standard procedure for determining the iodine number of activated carbon is outlined in ASTMD4607–94 (ASTM Standards, 2006). In a conical flask, 1 g of AC-1 powder was combined with 10 ml of 5 % of hydrochloric acid. The activated carbon was wetted by agitating the solution until the carbon was saturated. In a water bath, the mixture was heated for 30 s. After cooling the vessel to room temperature, 100 ml of 0.10 M iodine solution was added and gently shaken for 30 s. The liquid was filtered through paper cartridges. The filtrate was collected in a clean beaker and titrated until pale yellow against a 0.10 M sodium thiosulphate pentahydrate solution. To determine the level of concentration, a 0.40 M starch indicator was added, and titration continued until the blue color dissipated. This was performed three times to determine the mean value. The AC-2 and AC-3 granules, respectively, underwent the identical procedure.

2.5. Standard calibration curve for methylene blue

An inventory solution of methylene blue (MB) was prepared by dissolving 1.2 g of methylene blue dye in 1000 mL of distilled water and stirring it overnight with a magnetic stirrer to achieve uniformity. From the inventory solution, different diluted solution with the following concentrations: 1, 2, 3, 4, and 5 mg/L were prepared. The Eq. (8) was used to determine the appropriate volumetric volume of the standard working solution:

$$C_1V_1 = C_2V_2 \quad (8)$$

where C_1 is the concentration of the stock solution, V_1 is the volume to be transferred from the stock solution, C_2 is the concentration of the working standard solution and V_2 is the volumetric volume of the standard working solution. By determining the absorbance at 664 nm wavelength using UV/Vis Spectrophotometer, a calibration standard plot was created.

2.6. Effect of contact time

10 ml of Methylene blue solution of concentration of 250 mg/L was taken in 3 different conical flasks, to which 0.01 g of AC-1, AC-2 and AC-3 samples were added and shaken in a shaker at 115 rpm and 30 °C. The experiment was repeated for three times. Samples were collected at regular intervals for 1 h for 5 h and then after 24 h. The % absorbance at 664 nm was found out using a UV-spectrophotometer.

2.7. Batch adsorption experiments

Different concentrations of MB (10–250 mg/L) dye were prepared by dissolving pure dyes with distilled water. 10 mL aliquots of the prepared solutions were placed into five labeled 250 mL Erlenmeyer flasks, respectively. In each flask, 0.01 g of AC-1 powder was added, sealed with aluminum foil, and left to stand for 24 h at 30 ± 1 °C. After that, 5 mL of suspension was withdrawn. At a wavelength of 664 nm (which is the maximum absorption wavelength of MB), the absorbance of methylene blue was measured using a Tu-1901 UV/Vis spectrophotometer. The calibration curve was utilized to determine the solution's ultimate dye concentration. The percentage (%) removal of MB was based on Eq. (8) and adsorption capacity (Eq. (9)) as per the formula (Yaqubi et al., 2021). All test runs were carried out in triplicates for the reproducibility of the results. The same procedure was repeated for the AC-2 and AC-3 particles that had been sieved.

$$\text{MB removed (\%)} = \frac{(C_o - C_t)}{C_o} \times 100 \quad (9)$$

$$\text{Adsorption Capacity } (q_t)\ (\text{mg/g}) = \frac{(C_o - C_t)}{m} \times V \quad (10)$$

where C_o is the initial MB concentration at a time equal to zero of contact time in mg/L, C_t is the MB concentration at time t of the contact time in mg/L, V is the volume of the MB solution in (L) and m is the mass of the AC-1 added in grams. Equilibrium adsorption capacity, q_e (mg/g), is described by Eq. (11):

$$\text{Equilibrium adsorption capacity } (q_e)\ (\text{mg/g}) = \frac{(C_o - C_e)}{m} \times V \quad (11)$$

where C_e is dye concentration at equilibrium. The other parameters are described as above.

2.8. Adsorption kinetics

The kinetics of adsorption were studied at 30 °C. To comprehend the

characteristics of the dye adsorption process on AC-3, pseudo-first/second-order kinetic models have been used. The expression formulations were represented by Eqs. (12) and (13) (Yaqubi et al., 2021; Hung et al., 2022; Al. Haddabi et al., 2015).

$$q_t = q_e\left(1 - e^{-k_1 t}\right) \tag{12}$$

$$q_t = \frac{q_e^2 k_2 t}{1 + q_e k_2 t} \tag{13}$$

k_1 (min^{-1}) is the first order rate constant, and k_2 ($g.(mg.min)^{-1}$) is the rate constant of pseudo-second-order kinetic model.

The intraparticle diffusion model is based on the theory proposed by Morris and Weber, 1964 and is expressed in Eq. (14) as:

$$q_t = K_3 t^{1/2} + C \tag{14}$$

Where K_3 ($mg/g\ min^{1/2}$) is the intraparticle diffusion rate constant and C (mg/g) is a constant that gives an idea about the thickness of the boundary layer. A value of C close to zero indicates that diffusion is the only controlling step of the adsorption process.

2.9. Adsorption isotherms

Using the Langmuir and Freunlich isotherm models, equilibrium data were analyzed. This is how the Langmuir isotherm model was expressed (Ahmed and Dhedan, 2012):

$$q_e = \frac{q_{max} K_L C_e}{1 + L_L C_e} \tag{15}$$

where Ce (mg/L) is the equilibrium concentration of dye; qmax (mg/g) is maximum monolayer adsorption capacity; K_L (L/mg) is Langmuir equilibrium constant. The Langmuir isotherm model is investigated by separation coefficient R_L using Eq. (16) (Ahmed and Dhedan, 2012):

$$R_L = \frac{1}{1 + K_L C_o} \tag{16}$$

where the adsorption is favorable if $0 < R_L < 1$, unfavorable if $R_L > 1$, linear if $R_L = 1$ and irreversible if $R_L = 0$.

The Freundlich equation for heterogeneous surface systems was given by Eq. (8) (Ahmed and Dhedan, 2012):

$$q_e = K_F C_e^{1/n_F} \tag{17}$$

where K_F and n are Freundlich constants relating to the adsorption capacity and adsorption intensity, respectively. The magnitude of n gives an indication of the favorability of the process as values of $n > 1$ represent favorable adsorption.

The Sips isotherm model (Sips, 1948). is a combination of the Langmuir and Freundlich isotherm models and is expected to describe heterogeneous surfaces more accurately. At low adsorbate concentrations, the Sips isotherm approaches the Freundlich isotherm, whereas at high concentrations, it approaches the Langmuir isotherm (Ahmed and Dhedan, 2012). The model can be written as:

$$q_e = \frac{q_{max} K_s C_e^{1/m}}{1 + K_s C_e^{1/m}} \tag{18}$$

Where q_{max} (mg/g) is the maximum amount of MB adsorbed per unit mass of AC, K_S $(L/mg)^{1/m}$ is Sips constant related to energy of adsorption, and parameter m could be regarded as the parameter characterizing the system heterogeneity.

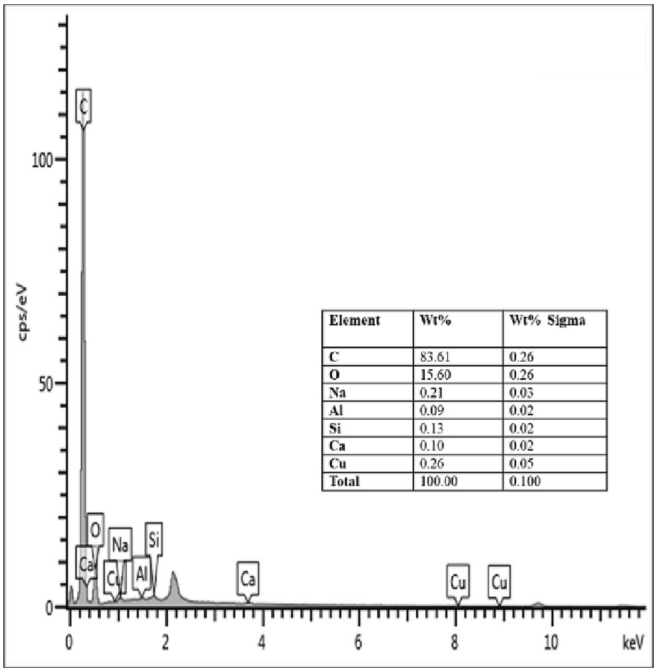

Element	Wt%	Wt% Sigma
C	83.61	0.26
O	15.60	0.26
Na	0.21	0.03
Al	0.09	0.02
Si	0.13	0.02
Ca	0.10	0.02
Cu	0.26	0.05
Total	100.00	0.100

Fig. 1. EDX spectrum and elemental analysis results (Table inset) of the prepared AC.

3. Results and discussion

3.1. Percentage (%) yield, ultimate analysis and morphological properties of prepared AC

The average AC production yield is 77.22 %. This result demonstrates that the acacia seedpod is a lignocellulosic material with a high cellulose content and a low lignin content, both of which are necessary for the formation of AC. The high yield of AC could be attributed to the H_3PO_4 as an impregnating reagent, where many carbons are removed as CO, CH_4, CO_2 and tar during the carbonization stage (Rashed, 2013).

Ultimate analysis results of the produced AC from *A. erioloba* seedpods with H_3PO_4 as the impregnating agent are presented in Fig. 1 (Fig. 1). EDX data highlight that the AC has a negligible number of metals such as Al, Si and Ca (≥ 0.13 %), low Cu and Na (≥0.26 %) content with a high carbon (83.61 %) and oxygen (15.60 %) contents. Hence, from the EDX it shows carbon as the dominant element among other elements. These results are comparable to some work on AC from *A. erioloba* seedpods using H_2SO_4 as an impregnating agent in which carbon content (82.09 %) was reported (Rahman et al., 2019). The elevated oxygen content of AC is a consequence of H_3PO_4 oxidation on the structure during heat treatment (Lupul et al., 2015).

SEM examined the AC's external and internal surfaces. Fig. 2 shows the resultant H_3PO_4-activated carbon microscope images.

The porous surface of the material is observable at higher magnification. The (a) and (b) SEM images show the pores in the micrometer diameter range. The material has a highly developed internal surface area and porosity, as well as a coarse texture and random cavities. These cavities are mesoporous according to IUPAC (Baig and Gul, 2021) standards and were the result of H_3PO_4 molecules evaporating during carbonization, leaving the spaces previously occupied by H_3PO_4 on the surface of AC, which leads to the formation of a porous, sponge-like material (Sher et al., 2020). On the surface of the AC, white particulates and impurities have formed due to the presence of H_3PO_4. This suggests that the acid introduced fissures to the surface of AC, resulting in a greater surface area (Molina-Sabio and Rodrıguez-Reinoso, 2004).

The BET method was employed to study the specific surface area (S_{BET}), the pore volume and the pore size, which reflect 387 m^2/g,

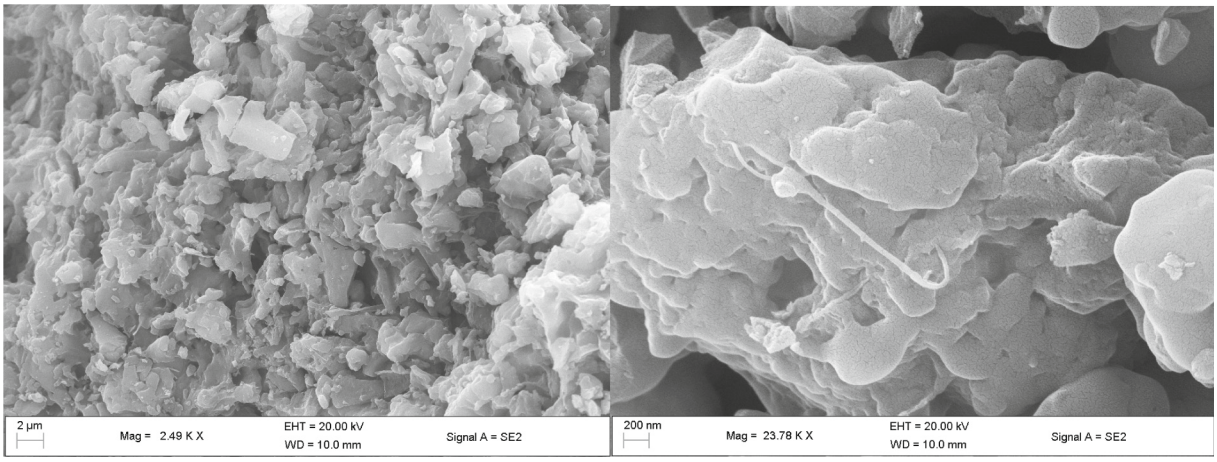

Fig. 2. SEM images of the (a) external and (b) internal of the prepared AC.

Table 2
Comparison of surface area, pore volume and pore size of produced AC to other studies with their activating agents.

Adsorbent	Activation agent	S_{BET} (m^2/g)	Pore volume cm^3/g	Pore size nm	References
Activated *A. erioloba* AC-500 °C/1 h)	H_3PO_4	387	0.208	1.76	This study
Activated *A. erioloba* seed pods (AC-600 °C/1 h)	H_2SO_4	362	0.040	39.58	Rahman et al., 2019
[a]CAC (Filtrasorb ®-400)	–	944	0.600	–	Saleem et al., 2017
[b]QAC-400	–	400	–	–	Saleem et al., 2017

[a] Calgon Carbon Corporation, Pennsylvania, 15205 USA.
[b] Quantum Active Carbon Pvt. Limited (2016).

0.2081 cm^3/g, and 1.76 nm, respectively. The S_{BET} agrees with most of the AC prepared by chemical activation (Rahman et al., 2019; 47; ASTM Standards, 2006). As adopted from the report of Udayakumar et al. (2021), the prepared AC powder in this study is microporous to mesoporous. The activating agent employed in this research effectively created well-developed pores leading to a large surface area and porous structure compared to H_2SO_4 that we reported previously (Rahman et al., 2019). It is known that H_3PO_4 develop large mesopores and macropores. KOH can only modify the microporosity to more heterogeneous micropores (Rivera-Utrilla et al., 2011). By comparing S_{BET} of prepared AC with the S_{BET} properties of two commercially available AC (Filtrasorb ®-400 and QAC-400) (Saleem et al., 2017) and AC S_{BET} information available in literature (*A. erioloba* seedpods with H_2SO_4 heat treated at 600 °C) (Rahman et al., 2019) are presented in Table 2.

Utilizing the BET method, the specific surface area (S_{BET}), pore volume, and pore dimension were determined to be 387 m^2/g, 0.2081 cm^3/g, and 1.76 nm, respectively. The S_{BET} concurs with most of the AC produced through chemical activation (Rahman et al., 2019; ASTM Standards, 2006). The AC granules produced via chemical activation have microporous to mesoporous [48]. The activating agent utilized in this study successfully generated well-developed mesopores, resulting in a large surface area and porous structure compared to H_2SO_4 (Rahman et al., 2019). It is understood that H_3PO_4 forms enormous mesopores and macropores (Lupul et al., 2015). Whereas KOH can only alter the microporosity to make it more heterogeneous (Saleem et al., 2017).

Table 3
The pH, moisture content, ash content, volatile matter, bulks density and fixed carbon of the prepared AC.

Determinant	AC-1	AC-2	AC-3
pH	8.8	8.56	8.50
% Moisture content	23.24	21.62	22.31
% Ash content	27.10	22.80	24.01
% Volatile content	21.50	22.85	22.50
% Fixed carbon	32.16	32.73	31.18

The AC's BET-surface area matches the results. Higher surface area means more adsorption platforms. AC shows higher adsorption capacity compared to AC prepared using the same precursor (*A. erioloba* seed pods) but changed the activation agent to H_2SO_4 (Rahman et al., 2019). BET-surface area is 40.1 % of CAC (Filtrasorb ®-400) (Saleem et al., 2017) and more than any other ACs (Rahman et al., 2019). Similar trends were observed in the obtained pore volume, which was approximately 35 % of CAC (Filtrasorb®-400) and greater than those of ACs (Rahman et al., 2019). H_3PO_4 dehydrates better than H_2SO_4 due to its activation method. This suggests that the produced AC is a realistic adsorbent, therefore local seed pods can meet the expanding demand for AC.

3.2. Proximate analysis of prepared AC sieved at a different size

For the proximate analysis, the prepared AC was sieved into various sizes, 50, 100 and 200 µm. The pH and percentages for moisture content, ash content, volatile matter, bulk density and fixed carbon of the produced AC-1, AC-2 and AC-3 are tabulated in Table 3.

Generally, the value of the power of hydrogen (pH) is one of the essential properties of an adsorbent that indicates its acidity/basicity of it and determines whether AC will develop a surface charge when submerged in an aqueous solution with a specific functional group. The prepared AC's pH indicates to be a weak basicity with a pH range of 8.5—8.8. The surface basicity of AC facilitates the adsorption of organic matter such as MB (Rivera-Utrilla et al., 2011).

For the produced AC-1, AC-2 and AC-3 samples, the moisture content was 23.24, 21.62 and 22.31 %, respectively. The moisture is due to various irregular porous characteristics (see SEM images Fig. 3), which can hold the water within. AC, with a large surface area and pore

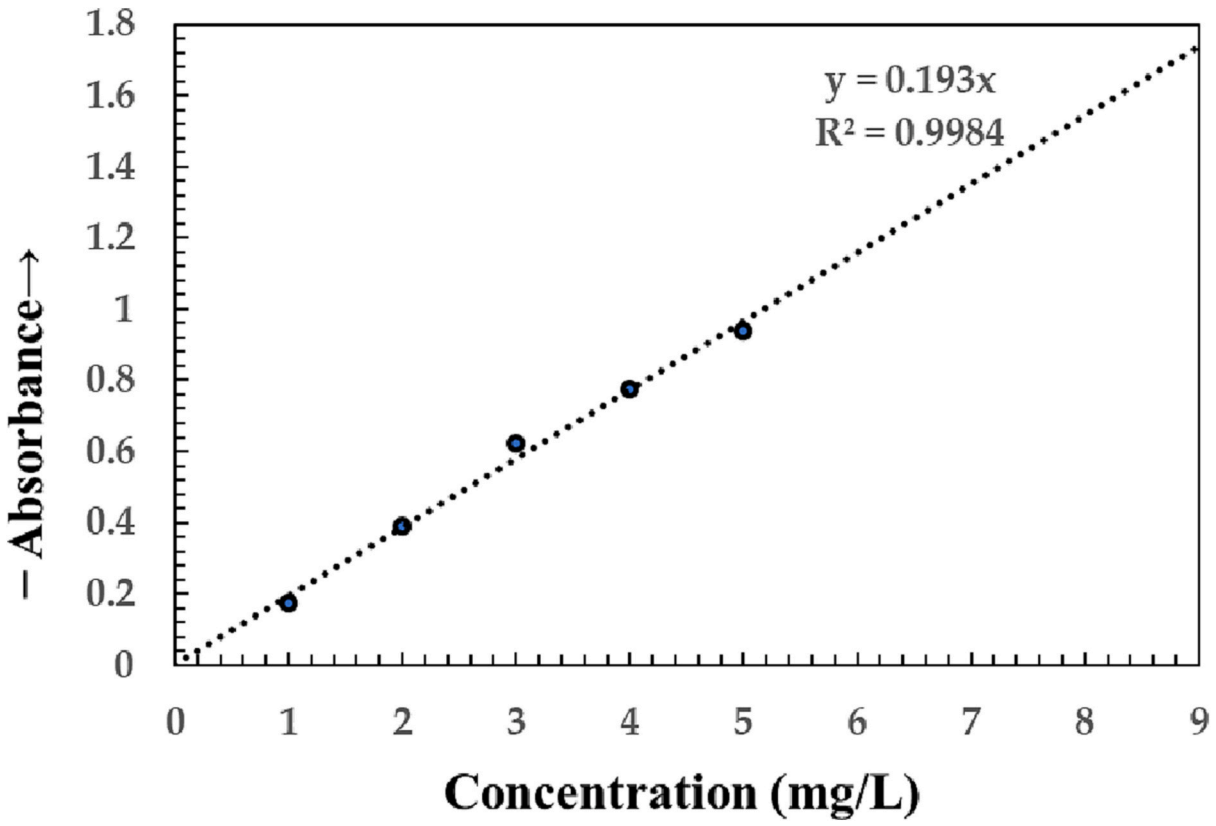

Fig. 3. Calibration plot for absorbance vs concentration (mg/L).

volume, will always adsorb moisture from the air unless preserved in airtight containers. AC-1, which has a 50 μm particle size, has the highest moisture content compared to other powders and a large surface area.

The ash content values represent the inorganic composition of the AC, thereby improving its hydrophilic qualities during the AC's regeneration due to catalytic actions. The ash content of the produced AC-1, AC-2 and AC-3 samples are 27.10, 22.80, and 24.01 %, respectively. High ash content could be due to the less efficient removal of impurities during the chemical activation followed by the pyrolysis of raw materials (Rahman et al., 2019). Generally, ash content above 10 % exhibits a larger surface area than low ash content (Zhang et al., 2020).

For the produced AC-1, AC-2 and AC-3 samples, the volatile content was 21.50, 22.85, and 22.50 %, respectively. For the produced AC samples, there is no significant difference between the volatile matters since all the carbon materials employed in this research were impregnated with 10 % of phosphoric acid. It is well known that as the percentage of activating agents increases, volatiles evaporate from the sample and yield decreases (Rivera-Utrilla et al., 2011). Usually, the volatile value of the samples generated from acacia plant materials is approximately 35 % (Rahman et al., 2019). The lower value of volatile % experienced in this project could be due to the decrease in holding time. The gasification time was 1 h. Increased adsorption time may result in the destruction of pore walls due to the increased evaporation of volatiles. Consequently, promote the widening of the micropores and converts them into mesopores (Liou, 2010; Hu et al., 2008).

Fixed carbon is the amount of non-volatile carbon remaining in a carbonaceous sample. The fixed carbon for the produced AC-1, AC-2 and AC-3 samples are 32.16, 32.73 and 31.18 %, respectively. Approximately 32 % of the prepared AC can be burned into a solid state, which is indeed beneficial to produce a higher yield of AC.

The bulk density provides insight into the floatability of the material. The bulk density for the produced AC-1, AC-2 and AC-3 samples are 0.58, 0.56, and 0.49 %, respectively, which means the activated carbon, will float in water, resulting in poor contact with the adsorbent, thereby consequence to a compromised adsorption process.

Table 4
Comparison of iodine number of prepared AC to another study with their activating agents.

Adsorbent	Activation agent	Iodine number (mg/g)	R^2	R^2_{adj}	References
Activated *A. erioloba* seed pods (AC-500/1 h)	H_3PO_4	AC-1 = 576 ± 2.6 AC-2 = 670 ± 2.4 AC-3 = 662 ± 2.9	AC-1 = 0.643 AC-2 = 0.583 AC-3 = 0.642	AC-1 = 0.286 AC-2 = 0.164 AC-3 = 0.285	This study
Activated *A. erioloba* seed pods (AC-600/1 h)	H_2SO_4	AC-1 = 528 ± 2.9 AC-2 = 638 ± 3.1 AC-3 = 554 ± 2.4	AC-1 = 0.629 AC-2 = 0.695 AC-3 = 0.358	AC-1 = 0.219 AC-2 = 0.299 AC-3 = 0.198	Rahman et al., 2019

3.3. Iodine number and number of pores of prepared AC

The iodine and MB indices were employed to estimate the microporosity and mesoporosity of the prepared ACs. The iodine number of prepared AC is presented in Table 4 and is compared with a study that used the same materials and procedure (Rahman et al., 2019), but

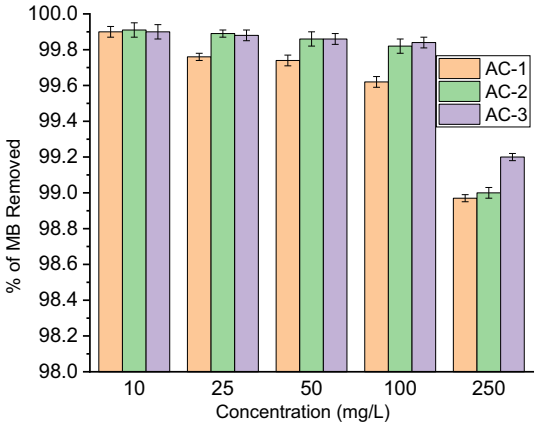

Fig. 4. Effect of adsorbent particle size (contact time 24 h, pH 7, temperature 30 °C).

changed only the impregnating agent to H_2SO_4.

Table 2 illustrates that the greatest iodine number is 670 mg/g for AC-2 sample generated using H_3PO_4. AC sucks out the 670 mg/g volume of impurities, which means the number of pores depends on the AC granule size and the impregnating agent employed. The other factor could be the preparation conditions (activation temperature, for example). It is well reported that the iodine number decreases with higher pyrolysis temperatures (> 500 °C) (Esfandiari et al., 2012). The AC samples prepared using H_2SO_4 were heat treated at 600 °C. The iodine number enhanced with increased activation temperature (Shaarani and Hameed, 2011). To validate the adequacy of the results, however, an ANOVA with a 95 % level of confidence was utilized. The variance analysis (ANOVA) tables containing the approximated iodine count are included in the appendix (Tables A1-A3). According to the ANOVA results, the equations did not sufficiently represent the correlation between each response and the significant data. This is also evident from the adjusted R^2 values in Table 2, which are far from 1, compared to the unadjusted values. Carbonization, activation, and impregnation temperatures lower the iodine number (Esfandiari et al., 2012).

3.4. Adsorption studies of prepared ACs

3.4.1. The calibration curve of methylene blue dye

Analyzing methylene blue in various solutions prior to and after adsorption is crucial for the adsorption study. The calibration curve of methylene blue dye was obtained at 664 nm is shown in Fig. 3 and was used for determining the concentration of dye in the solution at different MB concentrations after 24 h incubation.

The standard calibration curve depicts the linear relationship between the standard concentration of MB and the peak absorbance at 664 nm. The optical density = 0.193* concentration and R^2 = 0.998. The equilibrium concentration at time 't' was found by dividing the absorbance by the slope (Ce = (remaining concentration)/ (0.193)). The fact that the regression coefficient is >0.9 (R^2 = 0.998) indicates an outstanding linear fit in the concentration range considered initially. The Influence of contact time on dye removal by AC-3 is tabulated in Table A3.

3.4.2. The effect of initial dye concentration on the particles size of adsorbent

The adsorption properties of three samples, AC-1, AC-2, and AC-3, with particle sizes of 50 μm, 100 μm, and 200 μm, respectively, were compared based on their capacity to remove MB color compounds from aqueous solutions. The experiment was conducted for 24 h at varying MB concentrations (10, 25, 50, 100, and 250 mg/L) while maintaining

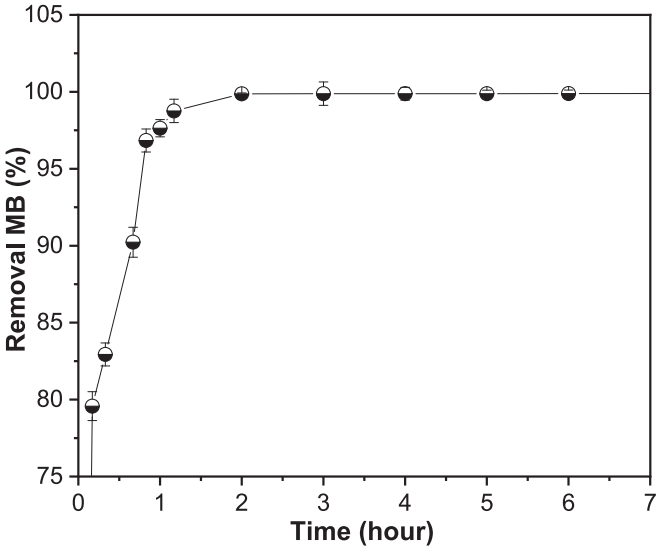

Fig. 5. Effect of contact time on the biosorption of MB onto AC-3.

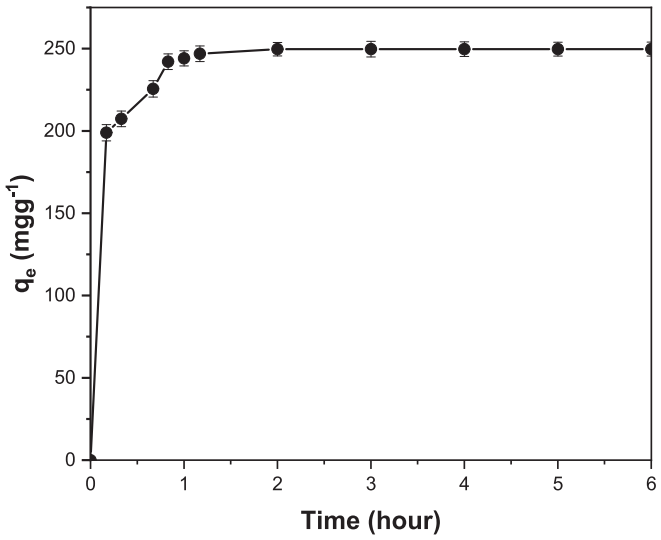

Fig. 6. Effect of contact time on MB adsorbed amount at 250 mg/L initial concentrations.
(dose = 0.01 g AC-3 in a 10 mL solution, pH = 7 at 30 °C).

constant pH (7.0) and temperature (30 °C). As shown in Fig. 4, the rate of MB removal decreases as the initial concentration of MB increases. At high concentrations, increased competition for sorption surface sites results in increased sorption rates. As anticipated, there is a trade-off between MB adsorption conversion and initial MB concentration. When the initial concentration of dye is increased, increasingly more molecules are absorbed by the surface of AC. Since the large quantity of adsorbed dye prevents direct contact with the pores of the adsorbent, this may have an inhibiting effect on dye adsorption. The MB concentration is reduced after 24 h, resulting in 99.9 % adsorption by all sizes of AC at low initial MB concentrations (10 mg/L), and 98.89 % adsorption at relatively higher initial MB concentrations (250 mg/L) of the dye solution. This suggests that the initial pollutant concentration is the dominant factor (Chen et al., 2022). The AC-3 sample removes the most MB at all concentrations, followed by AC-2 and then by AC-1. Consequently, the AC-3 sample was chosen for further testing.

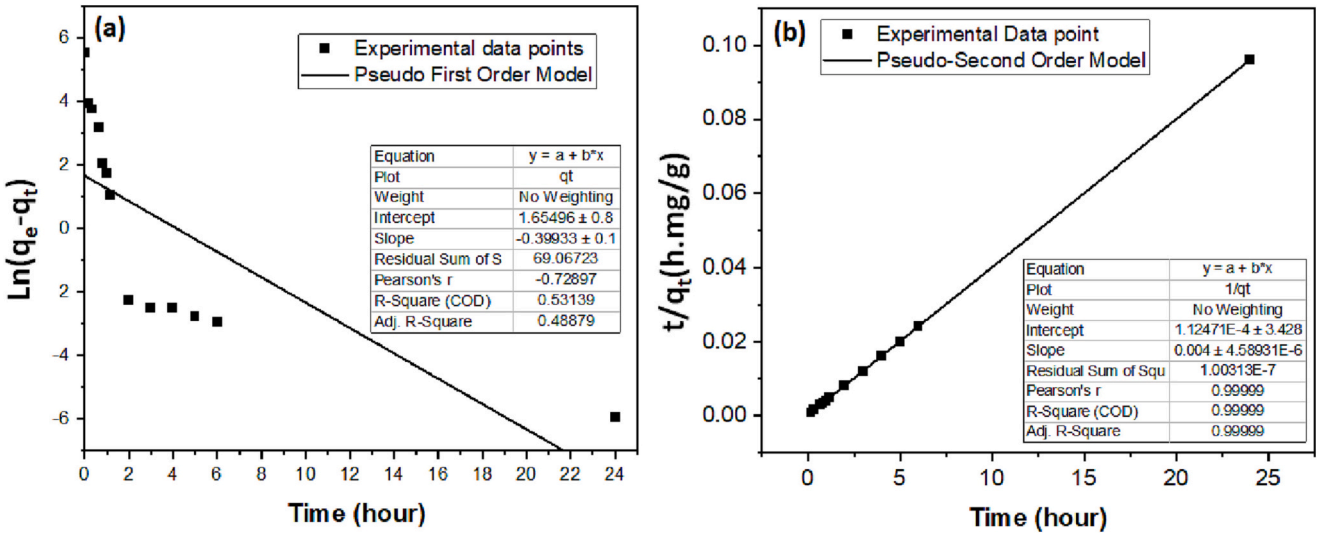

Fig. 7. (a) Pseudo-first order kinetic and (b) pseudo-second order kinetic for MB adsorption on AC-3. (dose = 0.01 g AC-3 in a 10 mL solution, pH = 7 at 30 °C). Symbols are experimental and lines are predicted data using respective kinetic models.

3.4.3. *The effect of initial concentration of dye solution on the percentage removal by AC-3 with contact time*

The effect of initial concentration (250 mg/L) of dye solution on the percentage removal was investigated at AC-3 dosage 0.01 g/10 ml of the dye solution for adsorption period of 6 h. The result is shown in Fig. 5. The removal of dye by adsorption onto AC was found to be rapid at the initial period of contact time, and then to become slow with the increase of contact time. Fast diffusion onto the external surface was followed by fast pore diffusion into the intraparticle matrix to attain rapid equilibrium (Hung et al., 2022).

3.4.4. *The adsorption capacity of AC-3*

Fig. 6 illustrates the investigation of the effect of contact time on the adsorption capacity of AC-3 for MB at 250 mg/L. This graph demonstrates that the quantity of MB adsorbed increases with increasing contact time, and equilibrium was reached in approximately 2 h. At a 2 h contact time, 7 pH value, and 0.01 g/10 mL adsorbent dose, the maximal adsorbed quantity (q_e) is 249.67 mg/g. This figure also indicates that a rapid increase in the quantity of MB absorbed occurs within the first hour. Because the force to transport MB ions is strong and the surface area of the particles and active sites are available for adsorption (Aroua et al., 2008), initial adsorption can occur rapidly. This phenomenon can be explained by the presence of many unbound adsorption sites in the initial phase, which facilitates the adsorption of dye molecules. When there are no available sites for adsorption, the dye molecules that are already on the AC surface repel the ones remaining in the solution (Hung et al., 2022; Yao et al., 2011), which makes the adsorption process slower.

3.4.5. *Adsorption kinetics*

To investigate the kinetics of the adsorption of 250 mg/L of initial MB dye onto 0.01 g of AC-3 in a 10 mL solution. The experimental kinetic data for MB adsorption on AC are fitted with pseudo-first order, pseudo-second order models, Eqs. (12)–(13), and presented in Fig. 7(a) and (b), respectively (El-Shafey et al., 2016; Yaqubi et al., 2021; Saleem et al., 2017; Al. Haddabi et al., 2015). Table 3 presents the calculated constants of the three isotherm equations and R^2 values at an initial MB concentration of 250 mg/L. As shown in Table 3, the R^2 values of the linear plot of $Ln(q_e-q_t)$ versus t (Fig. 7(a)) for pseudo-first order equation is low. This indicates a significant disparity between the experimental and calculated adsorption capacities, indicating an inadequate pseudo-first order fit to the experimental data. Table 3 displays high R^2 values for the linear plot of t/q_t versus t (Fig. 7(b)) for the pseudo-second order equation. The pseudo-second order kinetic model more accurately represented the adsorption kinetics, and the calculated q_e values (250 mg/g) match the experimental qe values (249.67 mg/g) (Table 5). The

Table 5
Kinetic parameters for MB adsorption on AC at 30 °C (dose = 0.01 g AC-3 in a 10 mL solution, pH = 7).

Kinetic model	C_0 (mg/L)	$q_{t,exp}$ (mg/g)	$q_{t,cal}$ (mg/g)	K_1 (1/min)	R^2_{adj}
Pseudo-first order	250	249.67	5.232	−0.0166	0.48879
				K_2 (1/min)	
Pseudo-second order	250	249.67	250	0.142	0.99999
			C (mg/g)	K_3 (mg/g $min^{1/2}$)	
Intraparticle diffusion	250	249.67	203.609	28.974	0.42401

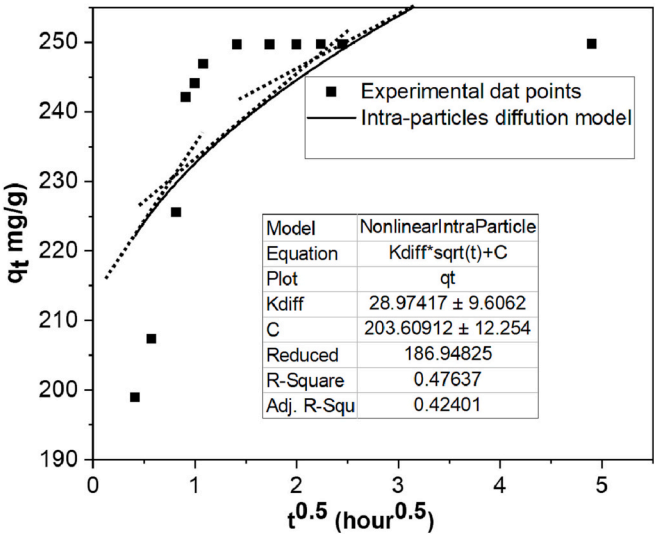

Fig. 8. Intraparticle diffusion plot for MB adsorption on AC-3 (dose = 0.01 g AC-3 in a 10 mL solution, pH = 7 at 30 °C). Symbols are experimental and lines are predicted data using intraparticle diffusion model.

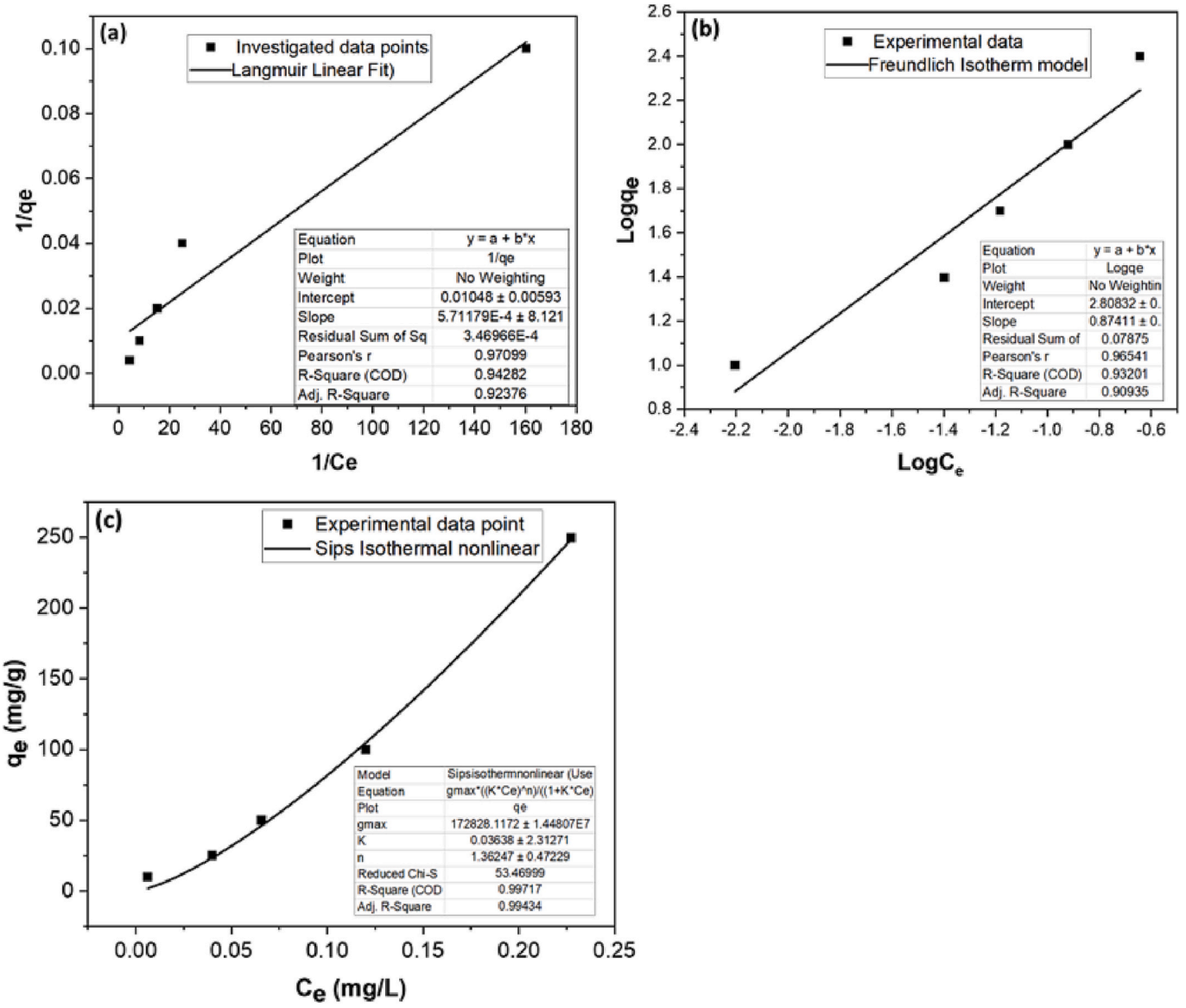

Fig. 9. Relationship between equilibrium MB concentration and its adsorption on on AC-3 (dose = 0.01 g AC-3 in a 10 mL solution, pH = 7 at 30 °C). Symbols are experimental and lines are predicted data using isotherm models.

observed data suggests that the adsorption of MB on AC can be described by a second-order kinetic model. During the research about MB absorption, Banat came across a fascinating discovery. They discovered a result that can be compared to their previous research on activated carbon from date stones, which was produced through physical activation using CO_2 (Banat et al., 2003). Ahmed and Dhedan (2012) discovered a comparable result while studying the adsorption of MB on date stone-derived activated carbon. As a means of chemical activation, zinc chloride was employed. The availability of adsorption sites, and not the concentration of dyes in solution, is the primary factor determining the adsorption rate (Tseng et al., 2006). Consequently, there were no statistically significant differences in the MB removal rate across concentrations. All removal rates of MB were higher than 98 % in Fig. 5.

The low values of R^2 (Table 3) for the nonlinear plot of q_t versus $t^{1/2}$ in Fig. 8 for the intraparticle diffusion model, calculated using Eq. (14), indicate that this model could not adequately fit the experimental kinetic data. This result is also consistent with other investigations (Hung et al., 2022; Ahmed and Dhedan, 2012) on the elimination of MB. Nevertheless, the intraparticle diffusion model can provide additional information regarding the diffusion mechanism and rate control stages (Chen et al., 2022). As depicted in Fig. 8, the curves of q_t on $t^{1/2}$ contain three linear segments, implying three MB adsorption processes by AC. In general, these three phases could be described as external diffusion, internal diffusion, and equilibrium (Wang et al., 2018). The initial stage is external diffusion, where the slope is steep and surface MB molecules diffuse from the solution system to the outer surface of AC molecules (Zhang et al., 2019). In the second stage, the MB molecules penetrate the AC molecules and bind to the internal active sites (Yu et al., 2020). The third stage is the equilibrium stage, in which the adsorption of MB molecules on AC decreases or even stops (Yang et al., 2020; Li et al., 2019). This may be a result of the decline in AC active sites. The concentration of residual MB is low, or electrostatic repulsion is increased (Chen et al., 2022). There are both physical and chemical adsorption processes occurring.

3.4.6. MB adsorption isotherms

The Sips model is an enhancement of the Langmuir and Freundlich models, and it possesses their characteristics (Serafin and Dziejarski, 2023). The experimental equilibrium data for MB adsorption on AC-3 are fitted with the Langmuir (Al. Haddabi et al., 2015; Li et al., 2019),

Table 6
Isotherm parameters for 250 ml initial concentration of MB adsorption on AC at 30 °C (dose = 0.01 g/10 mL, pH = 7, time = 24 h).

Isothermal model	Parameters	AC-3 (200 μm)
Langmuir	q_{max} (mg/g)	95.420
	K_L (L/mg)	0.183
	R_L	0.001
	R^2	0.924
Freundlich	n	1.144
	K_F(mg/g)(L/mg)$^{1/n}$)	643.16
	R^2	0.904
Sips	qmax (mg/g)	172,828.117
	Ks ((L/mg)$^{1/m}$)	0.036
	M	1.362
	R^2	0.994

Table 7
Comparison of MB maximum adsorption capacity (q_{max}) of onto activated carbon prepared from various precursors.

The precursor of AC (activator)	Maximum adsorption capacity (mg/g)	Ref.
Acacia erioloba seedpods (H_3PO_4)	95.42	This study
Corncob-activated carbon	0.84	Tseng et al., 2006
Acacia erioloba seedpods (H_2SO_4)	1.48	Rahman et al., 2019
Hazelnut shell	8.82	Aygün et al., 2003
Olive stones	22.10	Alaya et al., 2000
Waste apricot	102.00	Ahmed and Dhedan, 2012
Groundnut shell	164.90	Kannan and Sundaram, 2001
Commercial (Riedel DeHaën; item No.18001)	199.60	Djilani et al., 2015
Banana trunk waste-AC	227.27	Danish et al., 2018
Coffee husk	263.00	Oliveira et al., 2009
Oil palm fiber	277.78	Tan et al., 2007
Waste Elaeagnus stone	288.18	Geçgel et al., 2016
Pineapple waste	288.34	Mahamad et al., 2015
Durian shell	289.26	Chandra et al., 2007
Rattan sawdust	294.14	Hameed et al., 2007
Date stones	398.19	Ahmed and Dhedan, 2012
Peach stones	412.00	Attia et al., 2008
Vetiver roots	423.00	Altenor et al., 2009
Coconut husk	434.78	Tan et al., 2008
Bamboo	454.20	Doan (2023)
Longan seed	502.84	Hung et al., 2022
Sludge/coconut shell	602.80	Yang et al., 2019

Freundlich (Al. Haddabi et al., 2015), and Sips (Serafin and Dziejarski, 2023), using Eqs. (13), (14), and (15), respectively are plotted in Fig. 9. Table 6 presents the calculated parameters of the three isotherm equations along with their R^2 values.

Table 6 shows that for Langmuir isotherm, the value of separation factor (R_L) is less than one which favors the adsorption phenomenon (Itodo et al., 2010a, 2010b). This can also be concluded from the Freundlich model fitting results. The magnitude of the exponent, $1/n$ = 0.874, gives an indication of the favorability of adsorption. The adsorption intensity value of n > 1 represents favorable adsorption condition (Sivarajasekar and Baskar, 2014). This finding corresponds to a monolayer adsorption. The Langmuir model fitted the experimental data better than Freundlich model, indicating the adsorption of MB onto AC tended to monolayer adsorption. The sips model is found to best represent the equilibrium data with R^2 values of 0.994, suggesting the heterogeneous surface adsorption of MB on AC. The R^2 values of the three models descend in the order of: Sips > Langmuir > Freundlich. The results revealed that the equilibrium data are fitted by the three-parameter model rather than the two-parameter models. Several authors (Jang et al., 2019; Ahmed and Dhedan, 2012; Wang et al., 2018) showed the successful prediction of MB adsorption isotherm data using Sips isotherm as compared to Langmuir and Freundlich isotherms. This may be due to the ability of Sips isotherm to predict wide adsorbate concentration ranges. Therefore, the adsorption of AC by MB involves physical and chemical processes, same as the conclusions drawn from kinetic studies. Table 7 lists a comparison of MB adsorption capacity for the prepared activated carbon with those obtained in the literature.

Table 8
Langmuir of prepared AC compared to other studies.

Adsorbent	Activation agents	$S_{(Langmuir)}$ (m^2/g)	References
Activated *A. erioloba* seed pods (AC-500 °C/1 h)	H_3PO_4	AC-1 = 620 ± 5.0 AC-2 = 592 ± 2.6 AC-3 = 632 ± 3.6	This study
Activated *A. erioloba* seed pods (AC-600 °C/1 h)	H_2SO_4	AC-1 = 617 ± 4.1 AC-2 = 62 ± 3.6 AC-3 = 164 ± 2.9	Rahman et al., 2019

The surface area of AC was assessed further employing the Langmuir isotherm method (Sivarajasekar and Baskar, 2014). and compared to similar studies (Table 8). When H_2SO_4 is used for activation, the specific surface areas of AC with different particle sizes show a remarkable difference, whereas such phenomenon is not observed when H_3PO_4 is used. In the presence of H_3PO_4, the surface area increased significantly due to the small quantity of oxygen capabilities on the carbon surface, as determined by elementary analysis, as compared to H_2SO_4, which concurrently degraded or partially destroyed the porous structure (El-Hendawy, 2003). Moreover, H_2SO_4 samples were treated at higher temperature, 600 °C. Temperature treatment eradicated the surface's leftover oxidants (Qiao et al., 2002). This observation helps to understand why the absorption capacity of activated *A. erioloba* seed pods derived H_3PO_4 in this study was 90 folds higher than the activated *A. erioloba* seed pods derived-H_2SO_4. Therefore, AC can be considered as an efficient and low-cost alternative adsorbent for wastewater treatment, especially for the removal of organic dyes in water.

4. Conclusions

In conclusion, the produced AC can be produced from *A. erioloba* seedpods employing phosphoric acid as activating/impregnating agent. Compared to activation using H_2SO_4, H_3PO_4 proves superior in generating well-developed pores, leading to a mesoporosity and microporosity structure with a larger surface area. The iodine number of the produced AC was higher. The adsorption of MB on new AC material better fits with Langmuir's adsorption isotherm; hence, particles are adsorbed on well-pronounced heterogeneous surfaces. The sips model is found to best represent the equilibrium data with R^2 values of 0.994, suggesting the heterogeneous surface adsorption of MB on AC. Therefore, the adsorption of AC by MB involves physical and chemical processes, same as the conclusions drawn from kinetic studies. AC is an economical and eco-friendly green approach for wastewater treatment, notably for those in water-scarce nations such as Namibia. Specifically, the rising demand for activated carbon in Namibia can be met by producing inexpensive activated carbon from easily obtainable garbage materials, such as Acacia seedpods. The results suggest that adding prepared AC with H_3PO_4 is better than using H_2SO_4 as activator to raw water removes dissolved organic compounds. This results in a considerable requirement for AC application in wastewater treatment. This strategy will provide low-cost activated carbon and help with the bush encroachment problem in Namibia. Finally, new design methods need

additional research and development. New, promising AC materials must be integrated at higher technological levels to validate large-scale performance. ACs synthesis' small-scale practicality and performance do not guarantee reproducible upscaling.

CRediT authorship contribution statement

Conceptualization, A.R, V.U. and L.S.D.; methodology, H.M.N, P.K, S.B.J.; validation, H.N.M, A.R. and L.S.D.; formal analysis, A.R. and L.S.D.; investigation, H.M.N.; resources, A.R, and L.S.D; data curation, L.S.D; writing—original draft preparation, A.R and L.S.D.; writing—review and editing, L.S.D. and S.B.J.; supervision, A.R., V.U; project administration, A.R., V.U and L.S.D. All authors have read and agreed to the published version of the manuscript."

Funding

This research received external funding from National Commission Research Science and Technology (NCRST), under the call to strengthen research capacity at universities and research institutions (April 2017 to March 2022). Research project titled "Renewable Energy Initiative Project".

Institutional review board statement

Not applicable.

Informed consent statement

Not applicable.

Declaration of competing interest

The authors declare no conflict of interest.

Data availability

No data was used for the research described in the article.

Acknowledgements

Authors are grateful to the UNAM for providing support and facility to conduct this research and the Centre of Research Service (CRS) for providing technical help and support.

Appendix A. Supplementary data

Table A1: Analysis of variance for iodine number AC-1, Table A2: Analysis of variance for iodine number AC-2, Table A3: Analysis of variance for iodine number AC-3, Table B1: Percent removal of methylene blue by AC-1 (10 mg), Table B2: Percent removal of methylene blue by AC-2 (10 mg), Table B3: Percent removal of methylene blue by AC-3 (10 mg), Table C1: Contact time study data for AC-3, Table C2. Kinetic data for MB removal by AC-3 (10 mg) for Pseudo First order, Table C3: Kinetic data for MB removal by AC-3 (10 mg) for Pseudo Second order, Table C4. Kinetic data for MB removal by AC-3 (10 mg) for Intra-particles diffusion, Table D1. Isotherm data for MB removal by AC-2 (10 mg) for Langmuir adsorption isotherm, Table D2. Isotherm data for MB removal by AC-3 (10 mg) for Freundlich adsorption isotherm, Table D3. Isotherm data for AC-3 for Sips adsorption isotherm and Table E1: BET Print out as received. Supplementary data to this article can be found online at https://doi.org/10.1016/j.biteb.2023.101568.

References

Ahmed, M.J., Dhedan, S.K., 2012. Equilibrium isotherms and kinetics modeling of methylene blue adsorption on agricultural wastes-based activated carbons. Fluid Phase Equilib. 317, 9–14. https://doi.org/10.1016/j.fluid.2011.12.026.

Al. Haddabi, M., Vuthaluru, H., Znad, H., Ahmed, M., 2015. Removal of dissolved organic carbon from oily produced water by adsorption onto date seeds: equilibrium, kinetic, and thermodynamic studies. Water Air Soil Pollut. 226, 1–15. https://doi.org/10.1007/s11270-015-2443-1.

Alaya, M.N., Hourieh, M.A., Youssef, A.M., El-Sejariah, F., 2000. Adsorption properties of activated carbons prepared from olive stones by chemical and physical activation. Adsorpt. Sci. Technol. 18 (1), 27–42. https://doi.org/10.1260/0263617001493251.

Altenor, S., Carene, B., Emmanuel, E., Lambert, J., Ehrhardt, J.J., Gaspard, S., 2009. Adsorption studies of methylene blue and phenol onto vetiver roots activated carbon prepared by chemical activation. J. Hazard. Mater. 165 (1–3), 1029–1039. https://doi.org/10.1016/j.jhazmat.2008.10.133.

Aroua, M.K., Leong, S.P.P., Teo, L.Y., Yin, C.Y., Daud, W.M.A.W., 2008. Real-time determination of kinetics of adsorption of lead (II) onto palm shell-based activated carbon using ion selective electrode. Bioresour. Technol. 99 (13), 5786–5792. https://doi.org/10.1016/j.biortech.2007.10.010.

ASTM Standards, 2006. Designation D 4607-94, Standard TestMethod for Determination of Iodine Number of ActivatedCarbon. Designation D 2006, pp. 4607–4694.

Attia, A.A., Girgis, B.S., Fathy, N.A., 2008. Removal of methylene blue by carbons derived from peach stones by H3PO4 activation: batch and column studies. Dyes Pigments 76 (1), 282–289. https://doi.org/10.1016/j.dyepig.2006.08.039.

Ayelew, S., Mulualem, G., 2018. A review on bush encroachment's effect on cattle rearing in rangelands. J. Rangeland Sci. 8 (4), 403–415.

Aygün, A., Yenisoy-Karakaş, S., Duman, I., 2003. Production of granular activated carbon from fruit stones and nutshells and evaluation of their physical, chemical and adsorption properties. Microporous Mesoporous Mater. 66 (2–3), 189–195. https://doi.org/10.1016/j.micromeso.2003.08.028.

Baig, M.M., Gul, I.H., 2021. Conversion of wheat husk to high surface area activated carbon for energy storage in high-performance supercapacitors. Biomass Bioenergy 144, 105909. https://doi.org/10.1016/j.biombioe.2020.105909.

Banat, F., Al-Asheh, S., Makhadmeh, L., 2003. Preparation and examination of activated carbons from date pits impregnated with potassium hydroxide for the removal of methylene blue from aqueous solutions. Adsorpt. Sci. Technol. 21 (6), 597–606. https://doi.org/10.1260/026361703771953613.

Birch, C., Harper-Simmonds, L., Lindeque, P., Middleton, A., 2016. Benefits of bush control in Namibia. A national economic study for Namibia and a case for the Otjozondjupa Region. In: Report for the Economics of Land Degradation Initiative, 2016. Available from: www.eld-initiave.org.

Chandra, T.C., Mirna, M.M., Sudaryanto, Y., Ismadji, S.J.C.E.J., 2007. Adsorption of basic dye onto activated carbon prepared from durian shell: Studies of adsorption equilibrium and kinetics. Chem. Eng. J. 127 (1–3), 121–129. https://doi.org/10.1016/j.cej.2006.09.011.

Charis, G., Danha, G., Muzenda, E., 2019. Waste valorisation opportunities for bush encroacher biomass in savannah ecosystems: a comparative case analysis of Botswana and Namibia. Proc. Manuf. 35, 974–979. https://doi.org/10.1016/j.promfg.2019.06.044.

Chen, J., Li, J., Zeng, Q., Li, H., Chen, F., Hou, H., Lan, J., 2022. Efficient removal of tetracycline from aqueous solution by Mn-N-doped carbon aerogels: performance and mechanism. J. Mol. Liq. 358, 119153 https://doi.org/10.1016/j.molliq.2022.119153.

Danish, M., Ahmad, T., Majeed, S., Ahmad, M., Ziyang, L., Pin, Z., Iqubal, S.S., 2018. Use of banana trunk waste as activated carbon in scavenging methylene blue dye: kinetic, thermodynamic, and isotherm studies. Bioresour. Technol. Rep. 3, 127–137. https://doi.org/10.1016/j.biteb.2018.07.007.

De Wet, M.J., 2015. Harvesting Namibian encroacher bush: Compendium of harvesting technologies for encroacher bush in Namibia. Windhoek, Namibia: Support to De-Bushing Project, Deutsche Gesellschaft für Internationale Zusammenarbeit (GIZ) GmbH.

Dias, J.M., Alvim-Ferraz, M.C., Almeida, M.F., Rivera-Utrilla, J., Sánchez-Polo, M., 2007. Waste materials for activated carbon preparation and its use in aqueous-phase treatment: a review. J. Environ. Manag. 85 (4), 833–846. https://doi.org/10.1016/j.jenvman.2007.07.031.

Djilani, C., Zaghdoudi, R., Djazi, F., Bouchekima, B., Lallam, A., Modarressi, A., Rogalski, M., 2015. Adsorption of dyes on activated carbon prepared from apricot stones and commercial activated carbon. J. Taiwan Inst. Chem. Eng. 53, 112–121. https://doi.org/10.1016/j.jtice.2015.02.025.

Doan, L.H., 2023. Surface Modifications of Superparamagnetic Iron Oxide Nanoparticles with Polyvinyl Alcohol and Activated Charcoal as Methylene Blue Adsorbents. Available at SSRN 4409189. https://doi.org/10.2139/ssrn.4409189.

Duan, X., Srinivasakannan, C., Wang, X., Wang, F., Liu, X., 2017. Synthesis of activated carbon fibers from cotton by microwave induced H3PO4 activation. J. Taiwan Inst. Chem. Eng. 70, 374–381. https://doi.org/10.1016/j.jtice.2016.10.036.

El Gaayda, J., Titchou, F.E., Oukhrib, R., Karmal, I., Abou Oualid, H., Berisha, A., Akbour, R.A., 2022. Removal of cationic dye from coloured water by adsorption onto hematite-humic acid composite: experimental and theoretical studies. Sep. Purif. Technol. 288, 120607 https://doi.org/10.1016/j.seppur.2022.120607.

Eldridge, D.J., Bowker, M.A., Maestre, F.T., Roger, E., Reynolds, J.F., Whitford, W.G., 2011. Impacts of shrub encroachment on ecosystem structure and functioning: towards a global synthesis. Ecol. Lett. 14 (7), 709–722. https://doi.org/10.1111/j.1461-0248.2011.01630.x.

El-Hendawy, A.N.A., 2003. Influence of HNO3 oxidation on the structure and adsorptive properties of corncob-based activated carbon. Carbon 41 (4), 713–722. https://doi.org/10.1016/S0008-6223(03)00029-0.
El-Shafey, E.I., Ali, S.N., Al-Busafi, S., Al-Lawati, H.A., 2016. Preparation and characterisation of surface functionalised activated carbons from date palm leaflets and application for methylene blue removal. J. Environ. Chem. Eng. 4 (3), 2713–2724. https://doi.org/10.1016/j.jece.2016.05.015.
Esfandiari, A., Kaghazchi, T., Soleimani, M., 2012. Preparation and evaluation of activated carbons obtained by physical activation of polyethyleneterephthalate (PET) wastes. J. Taiwan Inst. Chem. Eng. 43 (4), 631–637. https://doi.org/10.1016/j.jtice.2012.02.002.
Geçgel, Ü., Üner, O., Gökara, G., Bayrak, Y., 2016. Adsorption of cationic dyes on activated carbon obtained from waste Elaeagnus stone. Adsorpt. Sci. Technol. 34 (9–10), 512–525. https://doi.org/10.1177/0263617416669727.
Gratuito, M.K.B., Panyathanmaporn, T., Chumnanklang, R.A., Sirinuntawittaya, N.B., Dutta, A., 2008. Production of activated carbon from coconut shell: optimisation using response surface methodology. Bioresour. Technol. 99 (11), 4887–4895. https://doi.org/10.1016/j.biortech.2007.09.042.
Hameed, B.H., Ahmad, A.L., Latiff, K.N.A., 2007. Adsorption of basic dye (methylene blue) onto activated carbon prepared from rattan sawdust. Dyes Pigments 75 (1), 143–149. https://doi.org/10.1016/j.dyepig.2006.05.039.
Hu, S., Xiang, J., Sun, L., Xu, M., Qiu, J., Fu, P., 2008. Characterization of char from rapid pyrolysis of rice husk. Fuel Process. Technol. 89 (11), 1096–1105. https://doi.org/10.1016/j.fuproc.2008.05.001.
Hung, N.V., Nguyet, B.T.M., Nghi, N.H., Thanh, N.M., Quyen, N.D.V., Nguyen, V.T., Khieu, D.Q., 2022. Highly effective adsorption of organic dyes from aqueous solutions on longan seed-derived activated carbon. Environ. Eng. Res. 28 (3), 220116 https://doi.org/10.4491/eer.2022.116.
Itodo, A.U., Abdulrahman, F.W., Hassan, L.G., Maigandi, S.A., Itodo, H.U., 2010a. Application of methylene blue and iodine adsorption in the measurement of specific surface area by four acid and salt treated activated carbons. N. Y. Sci. J. 3 (5), 25–33.
Itodo, A.U., Itodo, H.U., Gafar, M.K., 2010b. Estimation of specific surface area using Langmuir isotherm method. J. Appl. Sci. Environ. Manag. 14 (4) https://doi.org/10.4314/jasem.v14i4.63287.
Jagtoyen, M., 1996. Synthesis of Activated Carbons by the Phosphoric Acid Activation of Wood. University of Kentucky, Thesis.
Jang, E., Choi, S.W., Lee, K.B., 2019. Effect of carbonization temperature on the physical properties and CO2 adsorption behavior of petroleum coke-derived porous carbon. Fuel 248, 85–92. https://doi.org/10.1016/j.fuel.2019.03.051.
Jjagwe, J., Olupot, P.W., Menya, E., Kalibbala, H.M., 2021. Synthesis and application of granular activated carbon from biomass waste materials for water treatment: a review. J. Bioresour. Bioprod. 6 (4), 292–322. https://doi.org/10.1016/j.jobab.2021.03.003.
Joshi, R.R., 2015. Optimization of conditions for the preparation of activated carbon from Lapsi (Choerospondias axillaris) seed stone using ZnCl 2. J. Inst. Eng. 11 (1).
Kannan, N., Sundaram, M.M., 2001. Kinetics and mechanism of removal of methylene blue by adsorption on various carbons—a comparative study. Dyes Pigments 51 (1), 25–40. https://doi.org/10.1016/S0143-7208(01)00056-0.
Kutluay, S., Ece, M.S., Sahin, Ö., 2020. Synthesis of magnetic Fe3O4/AC nanoparticles and its application for the removal of gas-phase toluene by adsorption process. Int. J. Chem. Technol. 4 (2), 146–155. https://doi.org/10.32571/ijct.755732.
Li, Q., Wang, Z., He, Y., Sun, Q., Zhang, Y., Kumar, S., Cen, K., 2017. Pyrolysis characteristics and evolution of char structure during pulverized coal pyrolysis in drop tube furnace: influence of temperature. Energy Fuel 31 (5), 4799–4807. https://doi.org/10.1021/acs.energyfuels.7b00002.
Li, J., Li, B., Huang, H., Lv, X., Zhao, N., Guo, G., Zhang, D., 2019. Removal of phosphate from aqueous solution by dolomite-modified biochar derived from urban dewatered sewage sludge. Sci. Total Environ. 687, 460–469. https://doi.org/10.1016/j.scitotenv.2019.05.400.
Lim, W.C., Srinivasakannan, C., Balasubramanian, N., 2010. Activation of palm shells by phosphoric acid impregnation for high yielding activated carbon. J. Anal. Appl. Pyrolysis 88 (2), 181–186. https://doi.org/10.1016/j.jaap.2010.04.004.
Liou, T.H., 2010. Development of mesoporous structure and high adsorption capacity of biomass-based activated carbon by phosphoric acid and zinc chloride activation. Chem. Eng. J. 158 (2), 129–142. https://doi.org/10.1016/j.cej.2009.12.016.
Liu, S.L., Wang, Y.N., Lu, K.T., 2014. Preparation and pore characterization of activated carbon from Ma bamboo (Dendrocalamus latiflorus) by H 3 PO 4 chemical activation. J. Porous. Mater. 21, 459–466. https://doi.org/10.1007/s10934-014-9792-9.
Lupul, I., Yperman, J., Carleer, R., Gryglewicz, G., 2015. Tailoring of porous texture of hemp stem-based activated carbon produced by phosphoric acid activation in steam atmosphere. J. Porous. Mater. 22 (1), 283–289. https://doi.org/10.1007/s10934-014-9894-4.
Mahamad, M.N., Zaini, M.A.A., Zakaria, Z.A., 2015. Preparation and characterization of activated carbon from pineapple waste biomass for dye removal. Int. Biodeterior. Biodegradation 102, 274–280. https://doi.org/10.1016/j.ibiod.2015.03.009.
Mahari, W.A.W., Azwar, E., Foong, S.Y., Ahmed, A., Peng, W., Tabatabaei, M., Lam, S.S., 2021. Valorization of municipal wastes using co-pyrolysis for green energy production, energy security, and environmental sustainability: a review. Chem. Eng. J. 421, 129749 https://doi.org/10.1016/j.cej.2021.129749.
Mahmood, T., Ali, R., Naeem, A., Hamayun, M., Aslam, M., 2017. Potential of used Camellia sinensis leaves as precursor for activated carbon preparation by chemical activation with H3PO4; optimization using response surface methodology. Process. Saf. Environ. Prot. 109, 548–563. https://doi.org/10.1016/j.psep.2017.04.024.
Maquet, C., 2020. Wastewater reuse: a solution with a future. Field actions science reports. In: The Journal of Field Actions, 2020, Special Issue 22, pp. 64–69. http://journals.openedition.org/factsreports/6341.
Molina-Sabio, M., Rodrıguez-Reinoso, F., 2004. Role of chemical activation in the development of carbon porosity. Colloids Surf. A Physicochem. Eng. Asp. 241 (1–3), 15–25. https://doi.org/10.1016/j.colsurfa.2004.04.007.
Morris, J.C., Weber, J.R.W.J., 1964. Removal of biologically-resistant pollutants from waste waters by adsorption. In: Advances in Water Pollution Research. Pergamon, pp. 231–266.
Nahil, M.A., Williams, P.T., 2012. Pore characteristics of activated carbons from the phosphoric acid chemical activation of cotton stalks. Biomass Bioenergy 37, 142–149. https://doi.org/10.1016/j.biombioe.2011.12.019.
Oliveira, L.C., Pereira, E., Guimaraes, I.R., Vallone, A., Pereira, M., Mesquita, J.P., Sapag, K., 2009. Preparation of activated carbons from coffee husks utilizing FeCl3 and ZnCl2 as activating agents. J. Hazard. Mater. 165 (1–3), 87–94. https://doi.org/10.1016/j.jhazmat.2008.09.064.
Puziy, A.M., Poddubnaya, O.I., Gawdzik, B., Tascón, J.M.D., 2020. Phosphorus-containing carbons: preparation, properties and utilization. Carbon 157, 796–846. https://doi.org/10.1016/j.carbon.2019.10.018.
Qiao, W., Korai, Y., Mochida, I., Hori, Y., Maeda, T., 2002. Preparation of an activated carbon artifact: oxidative modification of coconut shell-based carbon to improve the strength. Carbon 40 (3), 351–358. https://doi.org/10.1016/S0008-6223(01)00110-5.
Rahman, A., Hango, H.J., Daniel, L.S., Uahengo, V., Jaime, S.J., Bhaskaruni, S.V., Jonnalagadda, S.B., 2019. Chemical preparation of activated carbon from Acacia erioloba seed pods using H2SO4 as impregnating agent for water treatment: an environmentally benevolent approach. J. Clean. Prod. 237, 117689 https://doi.org/10.1016/j.jclepro.2019.117689.
Rashed, M.N., 2013. Adsorption technique for the removal of organic pollutants from water and wastewater. Organ. Pollut. Monit. Risk Treat. 7, 167–194 (doi:105772/54048).
Rivera-Utrilla, J., Sánchez-Polo, M., Gómez-Serrano, V., Álvarez, P.M., Alvim-Ferraz, M.C.M., Dias, J.M., 2011. Activated carbon modifications to enhance its water treatment applications. An overview. J. Hazard. Mater. 187 (1–3), 1–23. https://doi.org/10.1016/j.jhazmat.2011.01.033.
Saleem, M., Ali, M., Siddiqi, Z., Al Qahtani, A.S., 2017. Preparation of activated carbon from acacia (Vachellia seyal) tree branches and application to treat wastewater containing methylene blue dye. Mod. Appl. Sci. 11 (12), 102–108. https://doi.org/10.5539/mas.v11n12p102.
Santoso, E., Ediati, R., Kusumawati, Y., Bahruji, H., Sulistiono, D.O., Prasetyoko, D., 2020. Review on recent advances of carbon based adsorbent for methylene blue removal from waste water. Mater. Today Chem. 16, 100233 https://doi.org/10.1016/j.mtchem.2019.100233.
Serafin, J., Dziejarski, B., 2023. Application of isotherms models and error functions in activated carbon CO2 sorption processes. Microporous Mesoporous Mater. 354, 112513 https://doi.org/10.1016/j.micromeso.2023.112513.
Seymour, C., Milton, S., 2003a. A collation and overview of research information on Acacia erioloba (camelthorn) and identification of relevant research gaps to inform protection of the species. Contract. 31 (2003/089).
Seymour, C., Milton, S., 2003b. A collation and overview of research information on Acacia erioloba (camelthorn) and identification of relevant research gaps to inform protection of the species. Contract 31 (2003/089) (Available from: https://cdn.24.co.za/files/Cms/General/d/7258/6ca73bb32e674a0b8179b6a89d0bf5a6.pdf).
Shaarani, F.W., Hameed, B.H., 2011. Ammonia-modified activated carbon for the adsorption of 2, 4-dichlorophenol. Chem. Eng. J. 169 (1–3), 180–185. https://doi.org/10.1016/j.cej.2011.03.002.
Sher, F., Iqbal, S.Z., Albazzaz, S., Ali, U., Mortari, D.A., Rashid, T., 2020. Development of biomass derived highly porous fast adsorbents for post-combustion CO2 capture. Fuel 282, 118506. https://doi.org/10.1016/j.fuel.2020.118506.
Shikangalah, R., Mapani, B., 2020. A review of bush encroachment in Namibia: from a problem to an opportunity? J. Rangeland Sci. 10 (3), 251–266. https://dorl.net/dor/20.1001.1.20089996.2020.10.3.4.3.
Shutova, Y., Rao, N.R.H., Zamyadi, A., Baker, A., Bridgeman, J., Lau, B., Henderson, R.K., 2020. Characterisation of dissolved organic matter to optimise powdered activated carbon and clarification removal efficiency. Environ. Sci. Water Res. Technol. 6 (8), 2065–2077. https://doi.org/10.1039/D0EW00149J.
Sips, R., 1948. On the structure of a catalyst surface. J. Chem. Phys. 16 (5), 490–495. https://doi.org/10.1063/1.1746922.
Sivarajasekar, N., Baskar, R., 2014. Adsorption of basic red 9 onto activated carbon derived from immature cotton seeds: isotherm studies and error analysis. Desalin. Water Treat. 52 (40–42), 7743–7765. https://doi.org/10.1080/19443994.2013.834518.
Song, M., Jin, B., Xiao, R., Yang, L., Wu, Y., Zhong, Z., Huang, Y., 2013. The comparison of two activation techniques to prepare activated carbon from corn cob. Biomass Bioenergy 48, 250–256. https://doi.org/10.1016/j.biombioe.2012.11.007.
Tan, I.A.W., Hameed, B.H., Ahmad, A.L., 2007. Equilibrium and kinetic studies on basic dye adsorption by oil palm fibre activated carbon. Chem. Eng. J. 127 (1–3), 111–119. https://doi.org/10.1016/j.cej.2006.09.010.
Tan, I.A.W., Ahmad, A.L., Hameed, B.H., 2008. Adsorption of basic dye on high-surface-area activated carbon prepared from coconut husk: Equilibrium, kinetic and thermodynamic studies. J. Hazard. Mater. 154 (1–3), 337–346. https://doi.org/10.1016/j.jhazmat.2007.10.031.
Tounsadi, H., Khalidi, A., Machrouhi, A., Farnane, M., Elmoubarki, R., Elhalil, A., Barka, N., 2016. Highly efficient activated carbon from Glebionis coronaria L. biomass: optimisation of preparation conditions and heavy metals removal using

experimental design approach. J. Environ. Chem. Eng. 4 (4), 4549–4564. https://doi.org/10.1016/j.jece.2016.10.020.
Tseng, R.L., Tseng, S.K., Wu, F.C., 2006. Preparation of high surface area carbons from Corncob with KOH etching plus CO2 gasification for the adsorption of dyes and phenols from water. Colloids Surf. A Physicochem. Eng. Asp. 279 (1–3), 69–78. https://doi.org/10.1016/j.colsurfa.2005.12.042.
Uchezuba, D.I., Mbai, S., Zimmermann, I., Bruwer, J., 2019. Investigating wood pellet torrefaction investment and its economic feasibility in the Krumhuk, Khomas region of Namibia. SN Appl. Sci. 1 (5), 402. https://doi.org/10.1007/s42452-019-0390-y.
Udayakumar, M., El Mrabate, B., Koos, T., Szemmelveisz, K., Kristaly, F., Lesko, M., Nemeth, Z., 2021. Synthesis of activated carbon foams with high specific surface area using polyurethane elastomer templates for effective removal of methylene blue. Arab. J. Chem. 14 (7), 103214 https://doi.org/10.1016/j.arabjc.2021.103214.
Van Auken, O.W., 2009. Causes and consequences of woody plant encroachment into western North American grasslands. J. Environ. Manag. 90 (10), 2931–2942. https://doi.org/10.1016/j.jenvman.2009.04.023.
Wang, H., Fang, C., Wang, Q., Chu, Y., Song, Y., Chen, Y., Xue, X., 2018. Sorption of tetracycline on biochar derived from rice straw and swine manure. RSC Adv. 8 (29), 16260–16268. https://doi.org/10.1039/C8RA01454J.
Yang, B., Liu, Y., Liang, Q., Chen, M., Ma, L., Li, L., Chen, Y., 2019. Evaluation of activated carbon synthesized by one-stage and two-stage co-pyrolysis from sludge and coconut shell. Ecotoxicol. Environ. Saf. 170, 722–731. https://doi.org/10.1016/j.ecoenv.2018.11.130.
Yang, Q., Wu, P., Liu, J., Rehman, S., Ahmed, Z., Ruan, B., Zhu, N., 2020. Batch interaction of emerging tetracycline contaminant with novel phosphoric acid activated corn straw porous carbon: Adsorption rate and nature of mechanism. Environ. Res. 181, 108899 https://doi.org/10.1016/j.envres.2019.108899.
Yao, Y., Bing, H., Feifei, X., Xiaofeng, C., 2011. Equilibrium and kinetic studies of methyl orange adsorption on multiwalled carbon nanotubes. Chem. Eng. J. 170 (1), 82–89. https://doi.org/10.1016/j.cej.2011.03.031.
Yaqubi, O., Tai, M.H., Mitra, D., Gerente, C., Neoh, K.G., Wang, C.H., Andres, Y., 2021. Adsorptive removal of tetracycline and amoxicillin from aqueous solution by leached carbon black waste and chitosan-carbon composite beads. J. Environ. Chem. Eng. 9 (1), 104988 https://doi.org/10.1016/j.jece.2020.104988.
Yu, H., Gu, L., Chen, L., Wen, H., Zhang, D., Tao, H., 2020. Activation of grapefruit derived biochar by its peel extracts and its performance for tetracycline removal. Bioresour. Technol. 316, 123971 https://doi.org/10.1016/j.biortech.2020.123971.
Zhang, P., Li, Y., Cao, Y., Han, L., 2019. Characteristics of tetracycline adsorption by cow manure biochar prepared at different pyrolysis temperatures. Bioresour. Technol. 285, 121348 https://doi.org/10.1016/j.biortech.2019.121348.
Zhang, Y., Song, X., Zhang, P., Gao, H., Ou, C., Kong, X., 2020. Production of activated carbons from four wastes via one-step activation and their applications in Pb2+ adsorption: insight of ash content. Chemosphere 245, 125587. https://doi.org/10.1016/j.chemosphere.2019.125587.